Investigation of electronic relaxation in a classic paramagnet by selective-excitation double-Mössbauer techniques: Theory and experiment

Bohdan Balko

Science and Technology Division, Institute for Defense Analyses, 1801 North Beauregard Street,
Alexandria, Virginia 22311
(Received 12 August 1985)

Time dependence of hyperfine interactions, such as that due to electronic spin relaxation, can be observed in Mössbauer transmission spectra and is generally investigated to obtain important information about structure and function of materials. However, relaxation effects in transmission spectra are often masked by inhomogeneous broadening. Also, completely different kinetic paths may lead to similar transmission spectra, making it difficult to interpret the underlying physics. These difficulties can be overcome by using selective-excitation double-Mössbauer (SEDM) techniques. Earlier work indicated that SEDM could be used to (1) determine unambiguously the existence of relaxation, (2) determine directly the kinetic paths of the relaxing system, and (3) measure the relaxation rates between the various relaxing electronic levels. In this paper, these predicted advantages of SEDM are examined theoretically and experimentally. SEDM line-shape theory in the presence of relaxation is developed and calculations using superoperator techniques are used to determine the effects of various physical parameters and experimental conditions on the SEDM spectra and their physical interpretation. As a test and application of the SEDM theory, experiments were performed on tris-(pyrrolidine)dithiocarbamate [Fe(III)], TPDC[Fe(III)], a classic paramagnetic system, already extensively studied by other investigators and thus constituting in our study a well-known "calibration" sample. The calculated spectra were compared to the experimental results at 5.4, 8, and 78 K in zero external field. We obtained a base relaxation rate of $\Omega = 5.24 \times 10^9$ sec^{-1} over the temperature range studied and determined kinetic paths not observed in this compound in previous transmission studies. Thus, SEDM provided new information about a well-known system. On the basis of our SEDM results we were able to determine the actual relaxation kinetics operating in the system at low temperatures and select between three completely different models which give similar theoretical transmission spectra and, therefore, cannot be distinguished by transmission studies alone. A comparison is made between the relaxation in TPDC [Fe(III)], a relatively strong coupling system, and ferrichrome A(FA), another Kramers-doublet paramagnetic system but with weaker coupling, which has been studied earlier by Mössbauer techniques.

I. INTRODUCTION

The dynamics of the interaction between nuclei and electrons has long been the subject of intensive investigation by nuclear and electronic resonance techniques. In particular, Mössbauer-effect (ME) spectroscopy is uniquely suited to such investigations because of the sensitivity of the spectra to the details of hyperfine interactions. Consequently, ME spectroscopy has been used to study many diverse dynamic phenomena.[1-16] (Some examples of dynamic phenomena studied with Mössbauer spectroscopy are the following: paramagnetic relaxation,[1-3] molecular diffusion and reorientation,[4,5] ferrofluid dynamics,[6] Jahn-Teller distortions,[7] electron hopping,[8,9] lattice fluctuations,[10] spin-lattice relaxations,[11,12] spin waves,[13] spin relaxation,[14] and critical fluctuations and magnetic ordering.[15,16]) Most of the experiments have been performed in the popular transmission geometry which, although relatively simple experimentally, produces spectra which are often difficult to interpret.

Thus, although time-dependent hyperfine interactions in solids have been studied by a number of investigators

using Mössbauer transmission techniques, there are still major problems encountered in the analysis of transmission spectra which could lead to misinterpretation of the underlying physics. Some of these problems arise because of the difficulty of separating relaxation effects from the other causes of line broadening[17-20] and because completely different kinetic paths may lead to similar transmission spectra,[21] making it difficult to determine the true kinetics, even in relatively simple systems. For example, the classical paramagnet ferrichrome A (FA) has been studied with Mössbauer transmission spectroscopy and also with ESR for some time,[22] but not until recently have the true dynamics been determined in enough detail[23,24] to obtain a close fit between experimental and calculated results.

Clearly, more sensitive and selective experimental techniques are desirable to sort out the various dynamic processes occurring in solid and molecular systems. Here we investigate the applicability and advantages of selective-excitation double-Mössbauer (SEDM) spectroscopy[25-27] to the study of time-dependent hyperfine interactions in general and apply the results to the investigation

of spin relaxation in the classic paramagnet *tris*-(pyrrolidine)dithiocarbamate[Fe(III)], TPDC[Fe(III)]. The work was motivated by the observation that SEDM allows a direct measurement of energy transfer in the solid, obviating the major problems with the transmission techniques, and thus reveals more details of the process under investigation.

The SEDM technique has already been used to obtain information about time-dependent effects in some materials[23,28-30] and the theory of the SEDM line shape under restrictive[25] and ideal[31-33] conditions has been developed. However, there has been no systematic investigation of the SEDM line shape under dynamic conditions and no comparison of theoretical and experimental results for a system whose dynamics (spin relaxation, etc.) have been well established. Thus, a theoretical study of the SEDM line shape and its comparison with the experimental spectra of a well-known system was considered a necessary step in the further development of the technique and its utilization for general investigations of time-dependent hyperfine interactions.

In the theoretical development we have used the superoperator theory of the differential scattering cross section, assuming a general interaction Hamiltonian and arbitrary electronic relaxation rates. In preparation for the analysis of experimental SEDM spectra, we have developed a dynamic theory of the SEDM line-shape applicable to thick scatterers. As a special case, a closed-form solution of the differential scattering cross section for the effective-field reversal or spin-flip model of paramagnetism was obtained. We have also extended previous calculations to scatterers of arbitrary thickness and with anisotropic relaxation rates, and have applied our new results to the analysis of the SEDM spectra of TPDC[Fe(III)], a high spin ferric Kramers-doublet paramagnetic system.

TPDC[Fe(III)] has been extensively studied by Mössbauer transmission techniques.[34] Using SEDM, we have determined the relaxation dynamics to be completely different from those deduced from transmission studies. The new results are due to the higher selectivity and discrimination available with SEDM and serve as an example of the advantages available with this technique for dynamic studies.

II. SEDM TECHNIQUE

The procedure for obtaining an SEDM spectrum has been discussed elsewhere.[25-27] The physical arrangement shown in Fig. 1(a) reveals the characteristic features of SEDM. Here the differential scattering cross section of the Mössbauer isotope is measured, instead of the absorption cross section, as in transmission experiments.

To accomplish this, two Doppler modulators are used to record the four recoilless events: (i) emission of photon γ_1, by the ^{57}Co source, (ii) absorption of the photon γ_1, by the ^{57}Fe nucleus in the material under investigation, (iii) subsequent reemission of another photon γ_2, and (iv) its absorption by the ^{57}Fe nucleus in the single-line analyzer. SEDM spectra for two different excitation energies are shown in Fig. 1(b) and the processes responsible for the spectral lines are depicted in the energy-level diagram in Fig. 1(c).
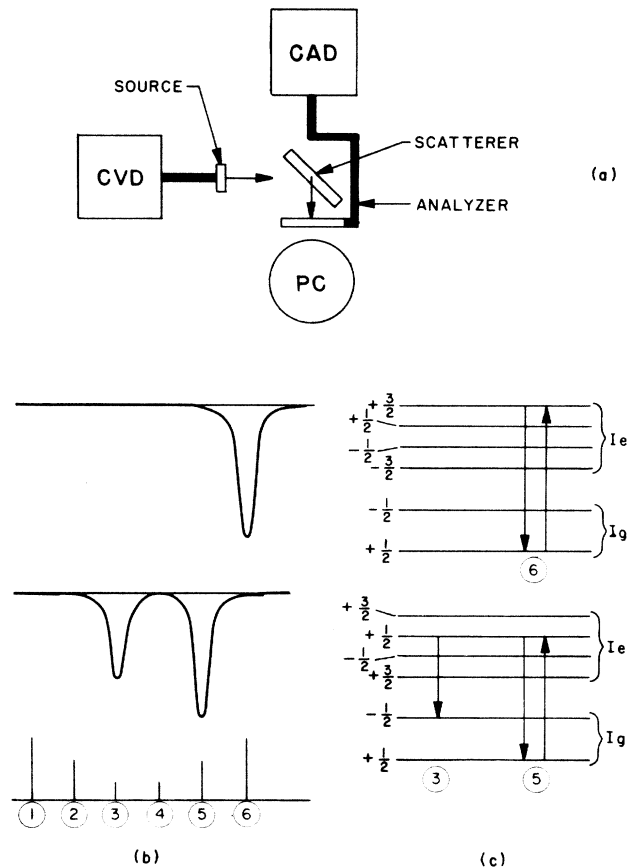
FIG. 1. Selective-excitation double-Mössbauer (SEDM) experiment and typical results: (a) experimental arrangement, (b) SEDM spectra obtained as a result of excitation of the fifth and sixth lines of a split ^{57}Fe scatterer, and (c) energy diagram of a magnetically split ^{57}Fe nucleus, showing the nuclear transitions participating in the scattering process observed in (b).

For comparison, the usual transmission spectroscopy would provide a spectrum of the same sample showing the six resonances as indicated by the stick diagram at the bottom of Fig. 1. Clearly, the transmission spectrum is more complex, exhibiting all the resonances of the system, while the SEDM spectrum shows only lines coupled to the specific resonance excited by the radiation from the source.

In transmission (and single drive scattering) experiments, the measured quantity is the absorption cross section, and the energy spectrum of the outgoing radiation is not determined. Consequently, information on the energy transformations in the scatterer during the lifetime of the nuclear state, which is contained in the energy of the scattered radiation, is not used. With the SEDM technique, the measured quantity is the differential scattering cross section, which is a function of the incoming and outgoing photon energies. Thus, the existence of relaxation in the scatterer, in the most propitious case, is explicitly exhibited in the SEDM spectrum by the appearance of lines at positions other than the excitation energy.[25-27] The exact

line shape depends on several factors, such as the relative magnitude of the various scattering cross sections in the material, the separation of the lines, the nuclear lifetime, and the relaxation rate. From an SEDM spectrum, one can obtain direct evidence for the occurrence of relaxation, measure the relaxation rate, and determine unambiguously between which lines the relaxation is occurring. Thus, from SEDM one can obtain detailed information about the kinetic mechanism operating in the system.[21,27] This important information has to be assumed when analyzing transmission data. The advantage inherent in the SEDM technique stems from the possibility of separating and identifying weaker components of the resonance system which would normally be concealed by stronger lines in a transmission spectrum.

There are many different applications of SEDM. (For example, SEDM can be used with advantage to search for small admixtures of nuclear states, such as that due to an electric quadrupole interaction,[35] to look for possible $E2$ transitions in the nuclear radiation spectrum,[36] or to unravel complex spectra consisting of several hyperfine patterns originating from inequivalent sites.[37]) In this paper, however, we concentrate on the study of relaxation processes in solids and biological molecules, where SEDM can be used to determine unequivocally the mechanism and rate of relaxation.

Hartmann-Boutron[32] has discussed the advantage of using SEDM in an investigation of slow relaxation. Balko and Hoy[25] have calculated results which clearly support this view (Ref. 25, Fig. 13). They show that for slow relaxation, the transmission spectra are characterized by a slight broadening of the line shape, which is difficult to distinguish from inhomogeneous broadening and thickness effects. In the SEDM spectra, on the other hand, the relaxation process is clearly identified by the appearance of lines away from the excitation energy. In another example of the application of SEDM to relaxation studies (Ref. 21, Fig. 3) two completely different modes of relaxation are differentiated and identified in an SEDM spectrum, while it is shown to be difficult, if not impossible, to separate out these processes using transmission spectroscopy.

With SEDM one can look at details of the relaxation processes. For example, it is possible to distinguish between perpendicular and parallel relaxation components, characterized by relaxation times T_1 and T_2 in nuclear magnetic resonance work, as discussed by Afanasev and Gorobchenko.[31] These authors propose hemin chloride as a particularly interesting example of a system in which it may be possible to obtain information about these relaxation times using SEDM. They point out that such information cannot easily be obtained from transmission studies.

Thus, SEDM can be used to (i) determine the existence of relaxation (or time-dependent hyperfine interactions) in a sample, (ii) determine in a direct way the kinetic paths of the relaxing system, and (iii) measure the relaxation rates between the various states of the system. In a relaxing system such as the classical paramagnet TPDC[Fe(III)], all of these determinations are required to establish the true dynamics.

III. SEDM LINE-SHAPE THEORY

The extraction of information from SEDM spectra on the time dependence of hyperfine interactions is predicted on two conditions. First, is the ability to predict the SEDM spectrum without relaxation occurring in the
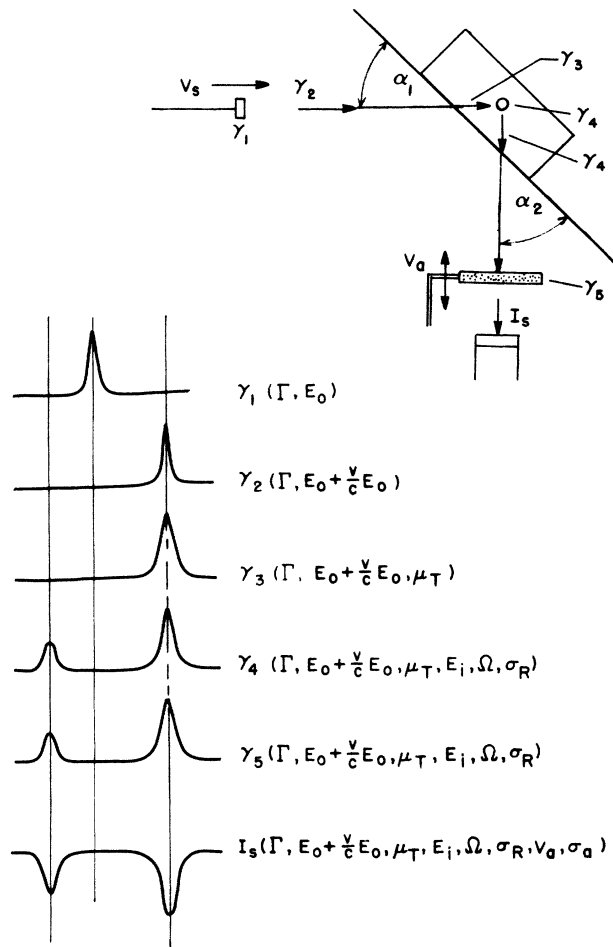
FIG. 2. Modification of photon-energy distribution by various processes occurring during an SEDM experiment. The SEDM geometry is shown in the upper-right-hand corner with α_1 and α_2 giving the directions of the incoming and outgoing photons. The various γ_i represent photon-energy distributions at different stages of the SEDM experiment. These distributions for an energy-transfer process involving two resonances are depicted in the figure. The functional dependencies of the energy spectra at various stages are also shown. γ_1 and γ_2 represent the photon energies emitted by the source and Doppler shifted by the constant velocity drive (CVD) respectively, γ_3 shows the photon modification due to incoherent thickness effects upon passage through the scatterer, γ_4 represents the emitted energy distribution after scattering by the ^{57}Fe nucleus, with second peak indicating relaxation (or magnetic dipole coupling), and γ_5 shows the incoherent thickness line-shape modification of the scattered beam. The SEDM line shape obtained after analysis with the single-line absorber is I_3, and is a function of the analyzer velocity V_a, the natural linewidth Γ, the total linear extinction coefficient for electronic absorption μ_T, the resonance energies E_i, the relaxation rate Ω, and the Rayleigh scattering cross section in the scatterer, as well as the analyzer thickness β.

scatterer, and in this way to determine the presence of relaxation by observing deviations from the predicted line shape. Second, is the ability to calculate the spectrum with time-dependent hyperfine interaction occurring in the scatterer to obtain kinetic and dynamic information by comparison of theory and experiment.

The calculation of the SEDM line shape without relaxation occurring in the scatterer has been treated extensively in the literature[25-27] and tested experimentally.[25,28] Studies of the various effects such as incoherent thickness,[25-27] Rayleigh and Mössbauer interference,[38] and multiple scattering and interference between different Mössbauer lines in the same nucleus[35,39] have been discussed before. Coherent thickness effects leading to Bragg scattering,[39,40] suppression of the inelastic channels, such as internal conversion[41,42] and the photoelectric cross section,[43] as well as superradiance,[44] are expected to be important only under special and well-defined conditions. Many of these effects are discussed in recent reviews on Mössbauer scattering.[42,45] In our discussion of the application of SEDM to relaxation, such coherent effects will not be considered.

Incoherent thickness effects, however, which are due to uncorrelated absorptions, are important for our consideration. A thick sample[38,46] effectively presents a broadened scattering cross section to the incoming beam, which results in the outgoing beam line shape closely resembling the incoming beam line shape. This observation holds for all thick scatterers and is independent of the details of the resonance structure of the scatterer (Ref. 27, Fig. 10). This result simplifies the analysis of SEDM spectra, because it guarantees that only relaxation (with the important exception of coupled or competing nuclear transitions) can shift lines, or in any significant way modify the line shape. The effect has been checked experimentally with several samples[27] and remains true even when the lines are inhomogeneously broadened.

The experimentally observed SEDM line also contains a Rayleigh component which is elastic, and consequently appears at the incoming beam energy. The Rayleigh contribution can be independently determined by a specially designed SEDM experiment[38] and simply included in the computation of the desired SEDM line shape.

The dynamic theory of the SEDM line shape, assuming a general interaction Hamiltonian and arbitrary electronic relaxation rates, has been developed by other investigators.[31-33] Their results, however, are restricted to thin scatterers $(\beta = n\sigma_0 f \cong 0$, where n is the number of ^{57}Fe nuclei per cm^2, σ_0 the maximum resonant absorption cross section, and f the recoilless fraction), and therefore cannot be applied to the analysis of experimental SEDM spectra in general because experiments are usually performed with thick scatterers $(\beta \geq 300)$. In the following we have extended the calculations to scatters of arbitrary thickness, in order to apply the results to the analysis of our experimental SEDM spectra.

The general calculation of the SEDM line shape must include all the processes affecting the propagating γ ray during the SEDM experiment, as depicted in Fig. 2. We consider a γ-ray beam emitted by a ^{57}Co source, scattered by a thick sample, partially absorbed by a single-line absorber (the Mössbauer analyzer), and finally detected at a particular scattering angle. Following the arguments leading up to Eq. (12) of Ref. 25, the energy distribution I of the radiation scattered by the sample can be written as

$$I(E',S) = I_M(E',S) + I_R(E',S), \tag{1}$$

where E' is the energy of the scattered radiation, S the resonance energy of the incoming beam, and I_M, I_R the Mössbauer and Rayleigh contributions, respectively. In Eq. (1) a 90° scattering geometry is assumed so that the interference term between the Rayleigh and Mössbauer components vanishes and the two intensities can be added. Following arguments similar to those used in Sec. III of Ref. 25 for the time-independent case, we can calculate the radiation scattered by a thick sample with a dynamic ^{57}Fe environment.

In terms of the differential scattering cross section, the intensity of the Mössbauer scattered radiation is given by

$$I_M(E',S) = I_0 \int_0^T dx \int_0^\infty dE \frac{d^2\sigma(E,E',\Omega)}{dE\,dE'} \exp\{-[\mu_T(E)\csc\alpha_1 x + \mu_T(E')\csc\alpha_2 x]\}, \tag{2}$$

where I_0 is the intensity of a narrow incoming beam, E and E' are, respectively, the energy parameters of the incoming and scattered beams, α_1 and α_2 are the directional angles of the incoming and outgoing beams as defined in Fig. 2, and $\mu_T(E)$ is the total linear extinction coefficient of the scatterer. The electronic part of $\mu_T(E)$ is considered independent of energy (for our purposes) (Ref. 25). The nuclear part, which is strongly dependent on energy, is given by

$$\mu_M(E) = nf\sigma_a(E,\Omega), \tag{3}$$

where n is the number of resonant nuclei per unit volume. Γ is the natural linewidth, and $\sigma_a(E,\Omega)$ is the absorption cross section of the scatterer. The cross section for a paramagnet in the effective-field approximation is well known (see, for example, Fig. 11 of Ref. 22). For other hyperfine interactions and a more realistic spin-relaxation model, the line shapes required by Eq. (3) can be quite complex. Some cases of special interest are given in Ref. 26.

The intensity of the scattered radiation is obtained from Eq. (2). In this expression the integration over x takes into account the absorption of the beam as it traverses the scatterer and can be easily performed. The integration over the incoming beam energy E, however, is not necessarily so trivial. In the stationary case, this integration can easily be carried out because all the energy-dependent terms are composed of Lorentzians.[25] In the time-dependent case this is not true and the integration, in general, has to be performed numerically. After a series of computations, we have determined that, to a good approximation (in most cases of interest), the line shape is not

appreciably affected if $\mu_T(E)$ is replaced by $\mu_T(S)$, the value of the extinction coefficient at the excitation energy. A comparison of results obtained with the correct but time-consuming integration procedure and the approximate computation showed that less than one-half percent error was introduced by the substitution. We therefore used this approximation in our numerical line-shape calculations.

Finally, taking into account the effect of the single-line absorber (or analyzer) attached to drive 2, the SEDM line shape is calculated from the energy distribution of the scattered radiation by

$$I(S,S') = \int_0^\infty I(E',S) e^{-\mu_a(E',S')T_a} \, dE', \tag{4}$$

where S' is the Doppler energy of the single-line absorber and

$$\mu_a(E',S') = \frac{\beta_a(\Gamma/2)^2}{[(E'-S'-E_0)^2 + (\Gamma/2)^2]T_a} . \tag{5}$$

The Mössbauer thickness of the absorber is $\beta_a = n_a \sigma_0 f_a$, where n_a is the number of ^{57}Fe nuclei per unit area and f_a is the recoilless fraction of the absorber, and T_a is the thickness of the absorber in centimeters.

Calculation of the SEDM line shape from Eqs. (1), (2), and (4) requires the determination of the differential scattering cross section, which will be discussed next. During the scattering process represented by Eq. (2), a Mössbauer nucleus undergoes a transition from a ground state g_1 to an excited state f, and then back to another ground state g_2, while a photon with wave vector k and energy E is absorbed and another photon characterized by k' and E' is emitted. Following Heitler[47] and Boyle and Hall,[48] we write the differential scattering cross section for this process as

$$\frac{d^2\sigma}{dE\,dE'} = \sum_{g_1,g_2} P_1 \left| \sum_f \frac{\langle k'g_2 | V | f \rangle \langle f | V | kg_1 \rangle}{[(E'-E) - \frac{1}{2}i\gamma][(E'-E_0) - \frac{1}{2}i\Gamma]} \right|^2 , \tag{6}$$

where V is the total interaction Hamiltonian between the nucleus and the radiation field, P_1 is the occupation probability of an initial state, and γ is the width of the ground state due to the incoming beam intensity.[48] For time-independent processes, the matrix elements in the numerator simply describe the strength of the scattering and the angular distribution through Clebsh-Gordan coefficients and vector spherical harmonics.[25]

For the analysis of dynamic processes, Eq. (6) can be rewritten by performing a Fourier transformation on the Lorentzian energy factors. Introducing the incoming beam linewidth Γ_b, and assuming an explicitly time-dependent Hamiltonian,

$$\frac{d^2\sigma}{dE\,dE'} = 2\,\mathrm{Re} \int_0^\infty dt \int_0^\infty dt_1 \int_0^\infty dt_2 [e^{i(E'-E)t - (\Gamma_b/2)t} e^{iE'(t-t_2) - \Gamma(t_1+t_2)/2} \langle V_k^{(+)} V_{k'}^{(-)}(t_2) V_k^{(+)}(t+t_1) V_k^{(-)}(t) \rangle]^{SA} \tag{7}$$

where

$$V_k^{(\pm)}(t) = \exp\left[i \int_0^t H(t')dt'\right] V^{(\pm)} \exp\left[-i \int_0^t H(t')dt'\right], \tag{8}$$

$V^{(\pm)}$ are the interaction operators for the nuclear emission and absorption and $H(t')$ is the time-dependent Hamiltonian for the nuclear-electronic system. (Banarjee[33] discusses the effect of relaxation on the polarization of the scattered radiation. Polarization is not measured in our SEDM experiment and therefore is not explicitly treated in this development.)

To obtain the SEDM line shape in the presence of relaxation, the stochastic average (SA) of the quantity inside the brackets in Eq. (7) has to be determined. In general, the stochastic and quantum-mechanical parts do not separate, and the average has to be taken together, as shown by Blume.[49] After time ordering is appropriately accounted for,[33] and introducing $t_3 = t + t_1$, Eq. (7) breaks up into three terms, with

$$\frac{d^2\sigma}{dE\,dE'} = 2\,\mathrm{Re}(I_1 + I_2 + I_3) \tag{9}$$

and

$$I_1 = \int_0^\infty dt_3 \int_0^{t_3} dt \int_0^t dt_2 [\ ]^{SA},$$

$$I_2 = \int_0^\infty dt_3 \int_0^{t_3} dt_2 \int_0^t dt[\ ]^{SA}, \tag{10}$$

$$I_3 = \int_0^\infty dt_2 \int_0^{t_2} dt_3 \int_0^{t_2} dt[\ ]^{SA} .$$

The brackets in Eq. (10) represent the stochastic averages of the time-dependent terms explicitly written out in Eq. (7). The correlation functions inside the brackets are most conveniently calculated using the Liouville superoperator approach.[49] This technique permits the calculation of the correlation function for all values of the hyperfine parameters and all relaxation rates. The time integration can also be easily performed. Several authors have discussed the evaluation of the SEDM line shape in terms of the integrals in Eq. (10) and have presented the results formally as functions of superoperators.[31-33]

Following the formalism of Afanasev and Gorobchenko,[31] the three terms in Eq. (9) comprising the scattering intensity of γ rays are given by

$$I_1 = J\{[\hat{A}_1 J'^\dagger] \hat{B} J' \hat{A}_2\} J^\dagger,$$

$$I_2 = J\{\hat{A}_3 [\hat{E}[A_1 J'^\dagger]J']\} J^\dagger, \tag{11}$$

$$I_3 = -J[\hat{E}[\hat{A}_1 J'^\dagger]J']\hat{A}_2\} J^\dagger .$$

In Eq. (11), J and $J^\dagger$ are the emission and absorption

operators, respectively, connecting the nuclear sublevels, and the superoperators A_1, A_2, A_3, B, and E are given by

$$\hat{A}_1 = \hat{G}_{eg}[iE' - \Gamma/2],$$

$$\hat{A}_2 = \hat{G}_{eg}[iE + (\Gamma + \Gamma_b)/2],$$

$$\hat{A}_3 = \hat{G}_{eg}[iE - (\Gamma + \Gamma_b)/2],$$ (12)

$$\hat{B} = \hat{G}_{gg}[i(E - E') + \Gamma_b/2],$$

$$\hat{E} = \hat{G}_{ee}[-i\Gamma],$$

where

$$\hat{G}_{\kappa\kappa'}(u) = \frac{1}{u - i\mathcal{H}^x_{\kappa\kappa'} + W}.$$ (13)

The Liouville operators $\mathcal{H}_{\kappa\kappa'}$ are defined by

$$\mathcal{H}^x_{\kappa\kappa'}a = \mathcal{H}_\kappa a - a\mathcal{H}_{\kappa'}.$$ (14)

In Eq. (14), $\mathcal{H}_\kappa, \mathcal{H}_{\kappa'}$ are Hamiltonians of the system in the extended space of nucleus and electrons, a is any operator in this space, and κ, κ', refer to the nuclear excited or ground substates, respectively.

Defining the states of the coupled atomic and nuclear system as $|v\rangle = |\psi_i, m_i\rangle$ and $|\mu\rangle = |\psi_f, m_f\rangle$ with ψ_i and ψ_f labeling the atomic states and m_i and m_f the nuclear states, respectively, we can write the matrix elements of the superoperators pertinent to the scattering problem in terms of the matrix elements of the excited and ground-state Hamiltonians as[49]

$$\langle\psi_f,m_g;\psi_i m_e \mid \mathcal{H}^x_{\kappa\kappa'} \mid \psi_f',m_g';\psi_i' m_e'\rangle = \langle\psi_f,m_g \mid \mathcal{H}_\kappa \mid \psi_f',m_g'\rangle \delta_{\psi_i,\psi_i'}\delta_{m_e,m_e'} - \langle\psi_i' m_e' \mid \mathcal{H}_{\kappa'} \mid \psi_i m_e\rangle\delta_{\psi_f,\psi_f'}\delta_{m_g,m_g'}.$$ (15)

In emission and absorption calculations (appropriate for transmission work) only the superoperator $\mathcal{H}^x_{eg}$, which connects the ground and excited states, appears. The matrix elements for this operator are written in an explicit notation in Ref. 24 with $m_f = m_g$ and $m_i = m_e$, the nuclear ground and excited states, respectively. For the scattering problem of interest here, the superoperators $\mathcal{H}^x_{ee}$ and $\mathcal{H}^x_{gg}$ are also required and can be computed from the general expressions, Eq. (15), with m_f and m_i representing both ground and excited state as required. In Eq. (13), W is the relaxation superoperator representing the interaction between the heat reservoir and the electrons. We treat this interaction in the white-noise approximation[50] so that W is independent of energy. The components of the superoperator W are functions of the transition matrix elements Ω_{ij} between electronic states i and j. The structure of the relaxation superoperator under these conditions is discussed by various authors[32,51] and the matrix elements for a particular model are explicitly written out in Ref. 24.

The superoperator expression for the scattering cross section in Eq. (7) is, in general, valid for all values of the hyperfine parameters and all relaxation rates. However, to obtain a solution for the line shape in all but the simplest cases is still a formidable computing problem because the superoperator approach involves computation of resonance denominators, which are functions of large matrices. In the limiting cases of high and low relaxation rates, Eq. (9) can be substantially simplified;[31] however, it is in the range of intermediate relaxation rates that most of the interesting phenomena occur, and it is this region that needs to be investigated.

For some special cases, such as in an effective-field approximation, the SEDM line-shape computation can be carried out analytically and the solution expressed in closed form as shown in the Appendix. The simplicity of this relaxation model allows one to follow the contribution of the various terms to the line shape as a function of relaxation rate. In particular, it is interesting to observe the appearance of the elastic peak at the excitation energy, and to study the difference between Raman scattering and hot luminescence.[52,53] The analytical solution is useful for gaining insight into the phenomena normally not available with a strictly numerical approach.

IV. CALCULATED RESULTS

In this section we present and discuss some sample SEDM spectra calculated from Eqs. (2) and (4) and the expressions developed in the Appendix for the effective-field model. These sample calculations were performed to gain insight into the relationship between SEDM spectra and the various physical parameters characterizing the scatterer, and to assess the information content of an SEDM spectrum under different conditions. Specifically, we were interested in determining the dependence of the SEDM line shape on (i) the relaxation rate Ω and electronic level population P_i, (ii) the Mössbauer thickness parameter β, which determines the inhomogeneous thickness effect, (iii) resonance Raman scattering and hot luminescence,[52,53] and (iv) different values for the transverse and longitudinal relaxation rates, Ω_1 and Ω_2.

Figure 3 shows some calculated SEDM spectra for two different scatterer thicknesses ($\beta = 10^{-3}$, $\beta = 500$) and two different excitation energies (fifth and sixth resonance lines in a split scatterer) as indicated by the vertical arrow, and for equal transverse and longitudinal relaxation rates ($\Omega_1 = \Omega_2 = \Omega$). The columns are labeled by Roman numerals and the rows by lower case letters. The relaxation rate Ω is given in units of the natural linewidth. The first column on the left (I) shows the resonance absorption cross section for a thin scatterer at various relaxation rates. The broadening of the lines and the collapse of the spectrum to a single central line in the motionally narrowed regime is typical of this type of relaxation.[22,24] These calculations were performed assuming a thin absorber, and consequently the observed line-shape modifications are strictly due to relaxation.

The second column (II) shows SEDM spectra calculated for excitation of the thin scatterer at line 6 (see Fig.1), while column III gives the SEDM spectra for the same excitation of the thick scatterer. Columns IV and V give

the calculated SEDM spectra for excitation of thin and thick scatterers, respectively, at the position of resonance, line 5. Notice that already for a low relaxation rate of $\Omega=0.5$, peaks at the positions of line 1 (columns II and IV) and line 2 (columns III and V) in the SEDM spectra are clearly visible, thus revealing the existence of relaxa-

tion in the sample. In the corresponding absorption cross sections (column I), the line broadening due to relaxation is not significant enough to demonstrate relaxation by transmission techniques until the relaxation rate is an order of magnitude higher. This shows that SEDM is clearly superior to transmission for investigating processes in
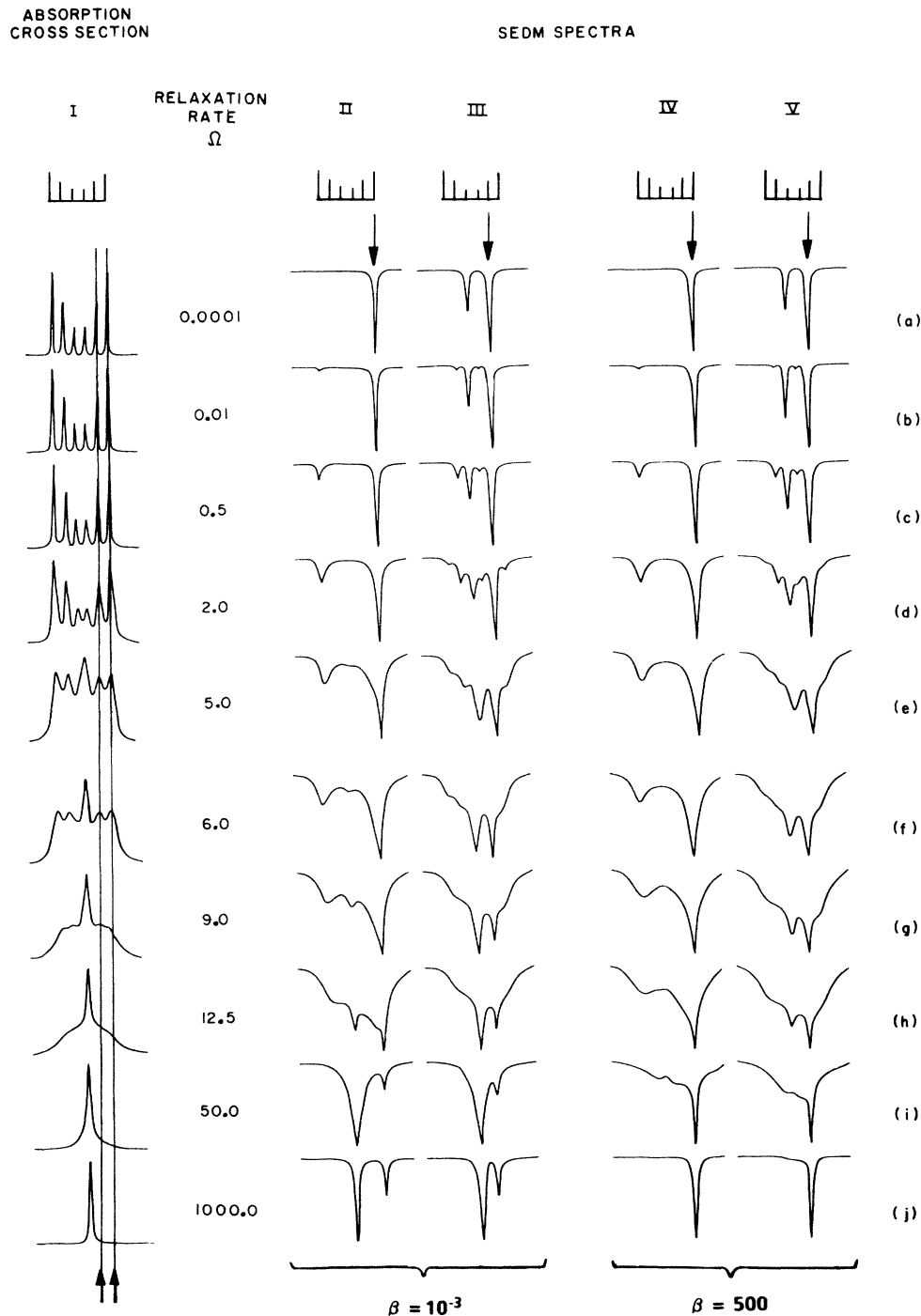
FIG. 3. Calculated SEDM spectra for a ^{57}Fe nucleus in iron metal in the presence of electronic relaxation approximated by a two-state effective-field model. Calculated results are shown for samples of Mössbauer thicknesses $\beta=10^{-3}$ and $\beta=500$, respectively, and two different excitation energies, as indicated by the vertical arrows. Column I shows the absorption cross section, columns II and III the results for excitation of the thin scatterer, and columns IV and V the results for excitation of the thick scatterer. Relaxation rates Ω, in units of the natural linewidth Γ, are given between columns I and II.

the slow relaxation regime.

It is also interesting to note that the difference in the normalized line shapes for thin and thick scatterers is insignificant until $\Omega = 5.0$, when the motionally narrowed central part of the absorption spectrum tends to "eat out" a peak in the thick scatterer due to the exponential thickness factor in Eq. (2). This difference becomes especially pronounced for higher relaxation rates. In the limit of large relaxation rates [for example, $\Omega = 1000.0$, row (j)] we find the same result previously obtained in the limit of low relaxation,[25] namely, that excitation of a line off resonance produces, in the SEDM spectrum of thin scatterers, two lines, one at the excitation energy and one at the scatterer resonance, but for thick scatterers this produces an SEDM spectrum showing only a single line at the excitation energy.

Note that the central line in row (j), columns II and III, is not due to a transfer of energy from the excitation peak to the central peak but is due to the overlap of two Lorentzians: the incoming beam profile with the motionally narrowed absorption cross section. How effectively this overlap is suppressed by the thickness factor depends on the excitation position (energy of the incoming γ ray) relative to the resonance, as can be seen by comparing row (j), columns IV and V.

The contribution to the SEDM spectrum from elastic nuclear scattering, and the distinction between the resonant Raman process and hot luminescence,[52,53] can be determined by considering the relative intensities of the

relaxation peak and the excitation peak. For example, in Fig. 3 [row (c), column II] for a relaxation rate $\Omega = 0.5$, the ratio of intensities of the relaxation peak to the excitation peak is $I_1/I_6 = 0.20$. According to a previous calculation[25] which included only the hot luminescent part, this ratio is given by $\Omega/(\Omega + \Gamma) = \frac{1}{3}$. The extra contribution to the peak at excitation in the calculation presented here comes from the resonant Raman process,[52,53] which was not included in the limited original theory but is included in the present superoperator calculation through term I_1 in Eq. (10). The effect of this purely nuclear process can also be observed at higher relaxation rates as a sharp peak at the excitation energy superimposed on a generally broader relaxation spectrum, as in the spectrum for $\Omega = 12.5$ shown in row h. [This peak is more prominent in Figs. 18 and 19 of Ref. 27, which shows the energy distribution of the scattered radiation and, thus, does not include the broadening effects of the analyzer constant acceleration drive (CAD) in Fig. 1(a).] Electronic Rayleigh scattering also contributes in a similar way, but the amount of contribution is constant.

Figure 4 shows calculated SEDM spectra for excitation of transition 4 [Fig. 1(a)] for different values of the transverse and longitudinal relaxation rates Ω_1 and Ω_2. From these calculations it is seen that increasing Ω_1 effectively increases the relaxation peaks and increasing Ω_2 broadens the lines of the SEDM spectrum. The two effects can, in principle, be distinguished in SEDM spectra, whereas as pointed out earlier by Afanasev and Gorobchenko[31] they are not distinguishable from transmission experiments.

V. EXPERIMENTAL

SEDM spectra of TPDC[Fe(III)] were obtained using an experimental arrangement similar to the one described in a previous paper.[25] The moving Mössbauer source consisted of 165 mCi of ^{57}Co in a rhodium matrix. The

FIG. 4. Calculated energy distribution of the scattered radiation (γ_5 in Fig. 2) assuming different longitudinal and transverse relaxation rates Ω_2 and Ω_1 of the electronic super relaxation matrix W. Only the inner four lines of the split ^{57}Fe spectrum (lines 2—5 in Fig. 1) are shown. The excitation energy is indicated in the figure by the vertical arrows.
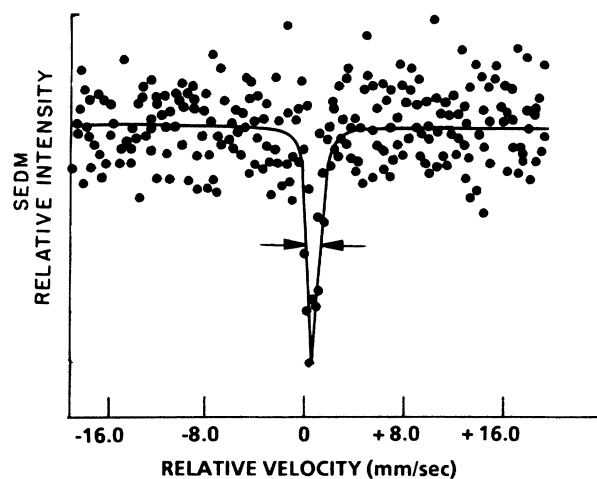
FIG. 5. An experimental SEDM spectrum of an iron bar with a natural content of ^{57}Fe obtained with the source stationary with respect to the scatterer.

TPDC[Fe(III)] polycrystalline sample was prepared according to the procedure described by Wickman and Wagner,[34] press-packed into a thin lucite dish 2.2 cm in diameter and covered with a 5-μm-thick sheet of plastic. The sample handling and mounting procedures were as described elsewhere.[25] Mössbauer transmission experiments were performed at several temperatures to check the quality of the sample. Our transmission spectra over the range of 5.4 to 78 K compared very well with previously published results,[24] testifying to the quality of the sample.

The SEDM experiments followed a procedure established earlier. First, we determined the maximum instrumental linewidth broadening, and the channel number corresponding to zero excitation velocity by performing an SEDM experiment on a bar of natural iron metal. The ^{57}Fe nuclei in the metal bar were excited off resonance so that the elastic scattering was predominantly due to the electronic Rayleigh scattering cross section. The result is shown in Fig. 5 and the maximum instrumental linewidth broadening determined from this is 0.23 mm/sec. A second set of experiments was performed on α-Fe$_2$O$_3$ (92% enriched in ^{57}Fe with a Mössbauer thickness β=240) to provide a check on instrumental broadening at

higher velocities and to determine the velocity calibration.

Experimental SEDM spectra of TPDC[Fe(III)] at three temperatures, 78, 5.4, and 8 K are shown in Figs. 6, 7, and 8, respectively. Each SEDM result is accompanied by a single-drive scattering spectrum,[46] which represents the absorption cross section at that temperature [Figs. 6(a), 7(a), and 8(a)]. Vertical arrows show the position of excitation by the constant velocity drive which resulted in the SEDM spectra shown at the bottom of the figures.

Figure 6 gives the results of experiments performed at 78 K. The spectrum shows that relaxation is occurring in the sample because there is a shift of the emitted spectral line from the position of excitation. A similar shift has been observed in earlier experiments on ferrichrome A (Ref. 21). For comparison, the dashed line gives the expected result, assuming no relaxation is present in the sample.

Figure 7 gives the results obtained at 5.4 K. The single-drive scattering spectrum, Fig. 7(a), shows a completely split pattern, although the broad lines imply a certain amount of relaxation in the sample. Excitation of line 6 results in the appearance of two lines in the SEDM spectrum [Fig. 7(b)], one at the position of excitation and the other, less intense, at the position of line 1. Clearly,
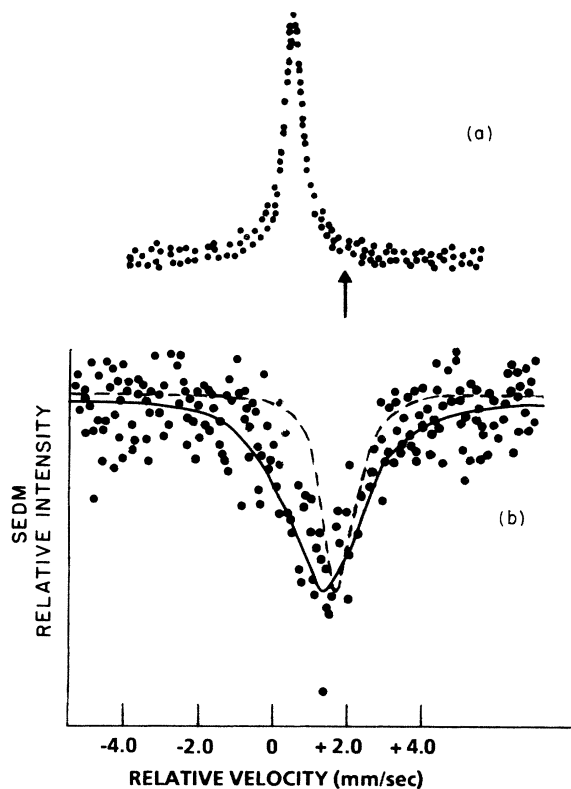
FIG. 6. Experimental Mössbauer spectra of TPDC[Fe(III)] taken at 78 K. The single-drive scattering spectrum is shown in (a) with the vertical arrow indicating the excitation energy for the SEDM experiments, the results of which are shown in (b). The solid line gives a theoretical spectrum, assuming the effective-field model with relaxation. The dashed line shows the calculated spectrum, assuming no relaxation occurring in the sample.
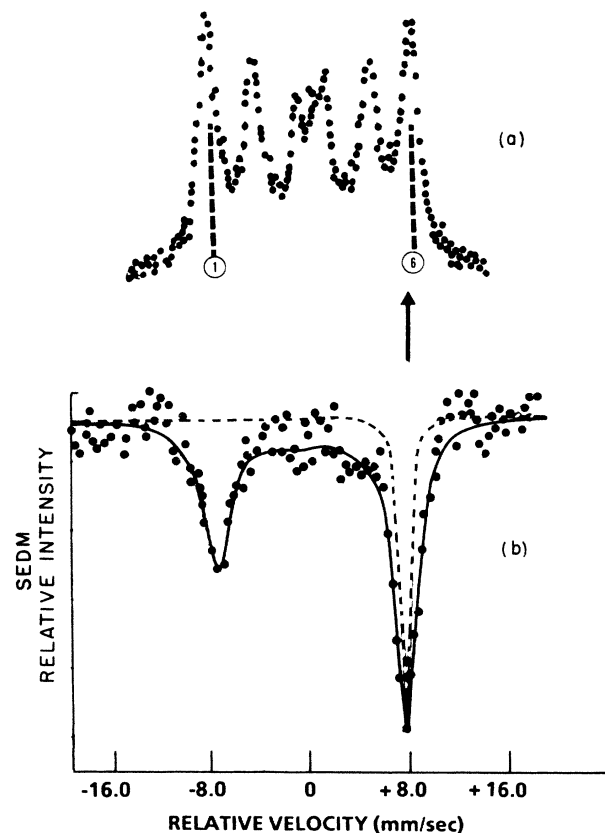
FIG. 7. Experimental Mössbauer spectra of TPDC[Fe(III)] taken at 5.4 K. The single-drive scattering spectrum is shown in (a) with the vertical arrow indicating the excitation energy for the SEDM experiment, the results of which are shown in (b). The solid line gives a theoretical spectrum assuming an effective-field model with relaxation. The dashed line shows the calculated spectrum, assuming no relaxation occurring in the sample.
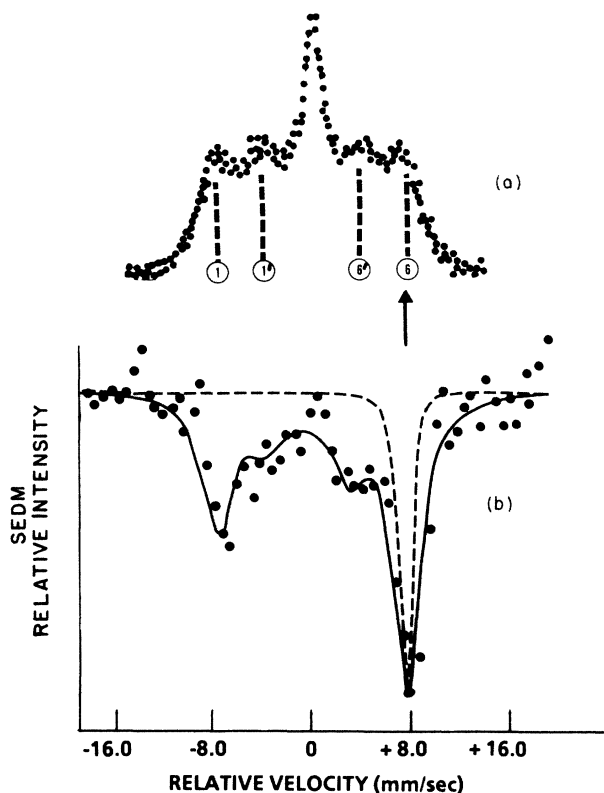
FIG. 8. Experimental Mössbauer spectra of TPDC[Fe(III)] taken at 8.0 K. The single-drive scattering spectrum is shown in (a) with the vertical arrow indicating the excitation energy for the SEDM experiment, results of which are shown in (b). The solid line gives a theoretical spectrum, assuming an effective-field model with relaxation. The dashed line shows the calculated spectrum, assuming no relaxation occurring in the sample.

an energy transfer due to relaxation is indicated, because the two lines in the SEDM spectrum are not connected by the magnetic dipole selection rule. Without relaxation, a single-line spectrum similar to the one observed after excitation of the sixth line in α-Fe_2O_3, would be expected, as in Fig. 1(b). Again, the dashed line in Fig. 7(b) gives the expected SEDM result, with no relaxation occurring in the sample, and reflects the experimental line broadening observed in the SEDM spectrum of natural iron metal (Fig. 5). The solid curve is a calculated SEDM spectrum using the theory presented in Sec. III and the relaxation model to be discussed in the next section.

Experimental results obtained with the sample at 8.0 K are shown in Fig. 8. The excitation energy for the SEDM experiment is indicated by the vertical arrow under the single drive scattering spectrum in Fig. 8(a). Excitation at this energy produces four lines in the SEDM spectrum, as shown in Fig. 8(b). The line at the excitation energy represents the sum of the elastic components of the scattered beam. The other lines are due to electronic relaxation processes occurring in the sample. This will be discussed in more detail in the next section. Again, the solid curve represents the calculated SEDM spectrum, including relaxation, as will be discussed in the next section.

VI. DISCUSSION

The theoretical SEDM line shapes calculated in Sec. IV for some selected hyperfine parameters, relaxation rates, and excitation energies indicate the rich information content of SEDM spectra. Similar calculations will now be used to analyze the SEDM spectra of TPDC[Fe(III)] in order to obtain the electron dynamics.

In TPDC[Fe(III)], the iron is in a structure surrounded by four sulfur atoms and a bidentate dithiocarbamate ligand. Wickman and Wagner[34] determined that unlike other similar compounds they studied, TPDC[Fe(III)] has a full Kramers electronic-level structure with a crystal-field Hamiltonian $H_{cf} = -DS_z^2$, $D = 2.1$ cm^{-1}, whence a ground state $S_z = \pm \frac{5}{2}$, an effective magnetic field of 540 kG in the ground level at liquid helium temperatures, and a small quadrupole splitting $E_Q = -0.035$ mm/sec. Mössbauer transmission experiments from 4 to 15 K show the complete range of paramagnetic spectra,[34] with a single motionally narrowed peak at 15 K and a completely split Zeeman pattern at 4 K. Our interest in this compound stems from the fact that it represents a perfect example of a simple paramagnetic structure as revealed by Mössbauer transmission spectra. With the small quadrupole splitting, the spectra are very symmetric and the whole pattern unfolds over an easily accessible temperature range.

Our initial reason for studying TPDC[Fe(III)] was to test in detail the SEDM superoperator line-shape theory on a well-known system. As this experimental work progressed, it became clear that SEDM revealed features of the electron dynamics that were not observed in earlier studies and that the relaxation in TPDC[Fe(III)] was not, therefore, actually well understood. In particular, the kinetic paths had not been correctly determined from the preceding experiments and the relaxation parameters Ω_{ij}, the quantities required to construct the relaxation supermatrix, were not known. We will show how these quantities can be determined from our SEDM spectra.

The SEDM spectra of TPDC[Fe(III)] shown in Figs. 6, 7, and 8, as well as Wickman's transmission spectra,[34] can be understood in terms of the high spin ferric model for the iron nuclear environment introduced by Hoy et al.[24] In this model the total Hamiltonian appropriate for describing high spin ferric compounds, such as TPDC[Fe(III)] and ferrichrome A, is given by

$$H = H_{cf} + H_{hyper} + H_n + H_{relax} , \qquad (16)$$

where the crystalline field spin Hamiltonian H_{cf}, the hyperfine Hamiltonian H_{hyper}, and the quadrupole interaction Hamiltonian H_n are given by

$$H_{cf} = D[S_z^2 - \tfrac{1}{3}S(S+1)] + E(S_x^2 + S_y^2) , \qquad (17)$$

$$H_{hyper} = A_z I_z S_z + A_x I_x S_x + A_y I_y S_y , \qquad (18)$$

$$H_n = \frac{e^2 qQ}{4I(2I-1)}[3I_z^2 - I(I+1) + (\eta/2)(I_+^2 + I_-^2)] . \qquad (19)$$

In Eq. (16), H_{relax} represents the relaxation interaction term which at low temperatures is assumed to be strictly

due to the dipole-dipole Hamiltonian

$$H_{d-d} = K^2 \sum_j \frac{1}{r_j^3} [\mathbf{S} \cdot \mathbf{S}_j - 3(\mathbf{S} \cdot \hat{\mathbf{r}}_j)(\mathbf{S}_j \cdot \hat{\mathbf{r}}_j)] , \qquad (20)$$

where S is the spin of the Mössbauer scattering ion and the index j extends over all the other ions separated from the ion of interest by r_j and with a spin direction θ_j. Our H_{relax} is the energy-conserving spin reversal term, term B, in Dattagupta's expansion of H_{d-d} given in Ref. 54,

$$B = -\tfrac{1}{4} K^2 \sum_j \frac{1}{r_j^3} (1 - 3\cos^2\theta_j)(S_+ S_{-j} + S_- S_{+j}) . \qquad (21)$$

The Hamiltonians H_{hyper} and H_n establish the nuclear-level structure shown in Fig. 9(a), which at low temperatures leads to six distinct lines in a Mössbauer transmission spectrum, 1 through 6 in Fig. 9(a). The Hamiltonian H_{cf} establishes an ionic-level structure as shown in Fig. 9(b).

Each Kramers doublet, although actually degenerate, is shown as two separate levels for clarity. The levels are labeled by their eigenvectors and in general

$$|\psi_i\rangle = a_1^i \,|\,\tfrac{5}{2},\tfrac{5}{2}\rangle + a_2^i \,|\,\tfrac{5}{2},\tfrac{3}{2}\rangle + a_3^i \,|\,\tfrac{5}{2},\tfrac{1}{2}\rangle + a_4^i \,|\,\tfrac{5}{2},-\tfrac{1}{2}\rangle$$
$$+ a_5^i \,|\,\tfrac{5}{2},-\tfrac{3}{2}\rangle + a_6^i \,|\,\tfrac{5}{2},-\tfrac{5}{2}\rangle , \qquad (22)$$

where the coefficients a_j^i are functions of $\lambda = E/D$ and, in particular, for $\lambda = 0$, $|\psi_i\rangle$ are pure magnetic quantum number states or $|\pm\tfrac{5}{2}\rangle$, $|\pm\tfrac{3}{2}\rangle$, $|\pm\tfrac{1}{2}\rangle$. The maximum admixture of states is produced when $\lambda = \tfrac{1}{3}$. The relaxation rates Ω_{ij} between the Kramers levels, derived from the dipole interaction Hamiltonian, are given by[24]

$$\Omega_{\text{if}} = \Omega(\,|\langle \psi_f | S_- | \psi_j \rangle|^2 + |\langle \psi_f | S_+ | \psi_i \rangle|^2)^2$$
$$\times \frac{\exp(-E_f/k_B T)}{\sum_k \exp(-E_k/k_B T)} , \qquad (23)$$

where $i \neq f$, and

$$\Omega_{ii} = - \sum_{\substack{f=1 \\ f \neq i}}^{6} \Omega_{\text{if}} .$$

This last relationship follows from detailed balance. In Eq. (23) k_B is the Boltzmann constant, ψ_i and ψ_f the initial and final electronic Kramers levels with E_i and E_f their respective energies, and Ω is the "bare" relaxation rate which is a function of the strength of the dipole-dipole interaction and includes the contribution from all ions as in Eq. (20). For a complete understanding of the electron-spin dynamics of a system, one has to determine experimentally the level structure and the relaxation rates Ω_{ij}.

It is convenient to introduce another parameter which is useful in comparing theoretical computations and experimental SEDM results. Thus, the effective relaxation rate

$$T_{\text{if}} = \frac{\Omega_{\text{if}}}{\Gamma + (P_i/P_f)\Omega_{\text{if}}} \qquad (24)$$

is a measure of the relative strength of the two competing processes for depopulation of the initially excited state $|\psi_i, I, I_z\rangle$, namely, the nuclear decay process and the electronic relaxation process represented by the linewidth Γ and the relaxation rate Ω_{if}, respectively. For relatively long nuclear lifetimes, such that Γ is small with respect to $(P_i/P_f)\Omega_{\text{if}}$, both the initial and final electronic-level populations will approach the equilibrium values given by the Boltzmann distribution. For relatively short nuclear lifetimes, such that Γ is large with respect to $(P_i/P_f)\Omega_{\text{if}}$, very little energy transfer between levels will take place.

The interplay between the static structural parameters D, E, and A and the dynamic parameters Ω_{ij} is often so involved that it is difficult, even for "simple" systems, to
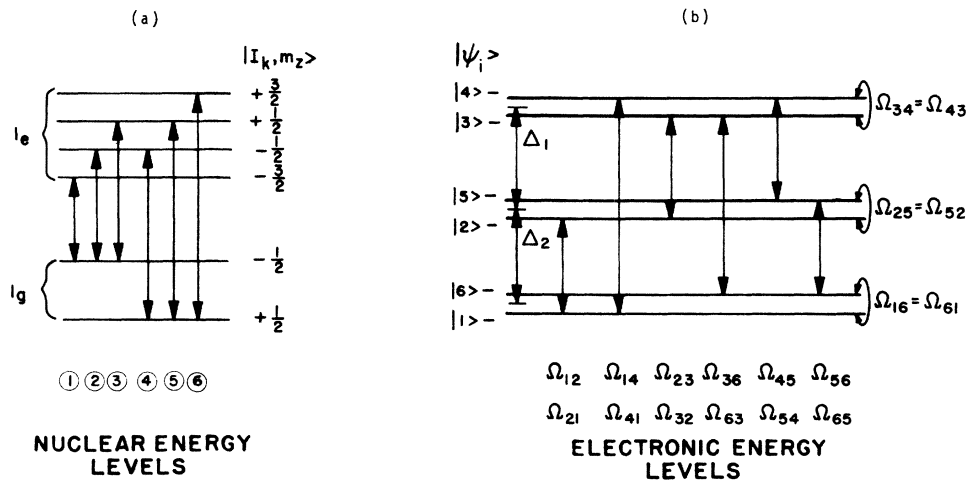
FIG. 9. Kramers-doublets-level scheme for high-spin ferric iron compounds like TPDC[Fe(III)] and ferrichrome A. (a) The nuclear energy levels are labeled by the magnetic quantum number and the allowed transitions are shown as lines $1 \to 6$. (b) The electronic levels are indicated by $|\psi_i\rangle = |1\rangle$ through $|6\rangle$, a notation which implies the generally mixed spin-state eigenfunctions of the iron ion. The doublets are actually degenerate in energy but for clarity are shown as split. The possible relaxation transitions from one electronic spin state $|i\rangle$ to another $|j\rangle$ are shown by vertical arrows and labeled by the relaxation rate Ω_{ij}.

generate a complete set of consistent spectra with the same set of parameters over a wide temperature range. This was only recently accomplished for ferrichrome A (FA) (Ref. 24) using the nonadiabatic Clauser-Blume relaxation theory. A good fit to experimental data over the complete temperature range of line-shape variability was obtained. (It should be noted that in this work with FA only the temperature was changed to generate the different spectra. All the other parameters were kept constant. Thus, there were no free parameters once the lowest temperature spectra were determined.)

When considering the difficulties involved in determining electronic kinetics from purely transmission results, it is interesting to note that the characteristic transmission spectra of TPDC[Fe(III)] shown in Fig. 4 of Ref. 34, as well as the single drive scattering spectra shown in Figs. 6(a), 7(a), and 8(a) can be fitted using theoretical models based on several completely different relaxation mechanisms. These mechanisms are (i) a simple effective-field flipping model (Ref. 22, Fig. 2), (ii) the Blume-Tjon effective-field model [Ref. 34, Fig. 4(b)], and (iii) the Clauser-Blume nonadiabatic spin-relaxation model with the asymmetry parameter (Ref. 24, Fig. 3) varying between $\lambda=0$ and a maximum value of $\lambda=\frac{1}{3}$. The models permit different kinetic paths and therefore give rise to different matrix elements of the relaxation matrix W. These paths are indicated by vertical arrows in Figs. 10(a)—10(c) for the transitions between electronic levels allowed by the three models. Since it is difficult on the basis of transmission and single drive scattering spectra to distinguish between such different kinetic paths, even for a simple system like TPDC[Fe(III)], one wonders about the conclusions reached from transmission results about the electron dynamics in more complex systems such as biological molecules.[2] This observation induced us to investigate the relaxation in TPDC[Fe(III)] with SEDM and to test our theoretical techniques on this well-studied system.

Let us consider the results of the SEDM experiments presented in Figs. 6, 7, and 8 in the theoretical framework of our spin-relaxation model. The SEDM spectrum shown in Fig. 6(b) indicates the presence of time-dependent effects by the shift of the scattered radiation from the excitation position. The dashed line gives the expected result for no relaxation, i.e., if, for example, the broad single-line spectrum were due to inhomogeneous broadening and not due to dynamic effects. The solid line is a calculated spectrum obtained from the dynamic model presented in Sec. III. (Input parameters for the theoretical calculations were obtained from the experimental conditions. With the exception of the normalization which was performed at the excitation peak, there were no other free parameters. The experimental line broadening was determined by fitting the calibration spectrum in Fig. 5 and the same value for the incoming beamwidth was then used in all the subsequent calculations.) In this high relaxation limit, it is difficult to distinguish relaxation rates Ω_{ij}, even with SEDM. However, at lower temperatures (and slower relaxation rates) the situation changes dramatically. The results at 5.4 and 8.0 K shown in Figs. 7 and 8, respectively, reveal new and interesting details about the relaxation dynamics. Excitation of the outermost line of the split spectrum shown in Fig. 7(a) results in two lines in the SEDM spectrum, one at the excitation energy, line 6, corresponding to the transition

$$| \psi_i;I,I_z \rangle = | 1;\tfrac{3}{2},\tfrac{3}{2} \rangle \rightarrow | 1;\tfrac{1}{2},\tfrac{1}{2} \rangle,$$

as shown in Fig. 10(a), and the other at the opposite end of the spectrum, corresponding to line 1 and the transition

$$| 6;\tfrac{3}{2},\tfrac{3}{2} \rangle \rightarrow | 6;\tfrac{1}{2},\tfrac{1}{2} \rangle.$$

The occurrence of the line at position 1 is directly related to a "spin-flip" relaxation in the ground Kramers doublet or $|1\rangle \rightleftarrows |6\rangle$. From a theoretical fit to this spectrum, we obtain a relaxation rate for the process of $\Omega_{16}=4.5$ in units of the natural linewidth Γ. This relaxation mechanism is schematically depicted in Fig. 10(c) where it is labeled mode A.

The results shown in Fig. 8(b) indicate another relaxation pathway [labeled mode B in Fig. 10(c)] operating in the sample at a temperature of 8.0 K. This mode transfers energy between the ground and intermediate
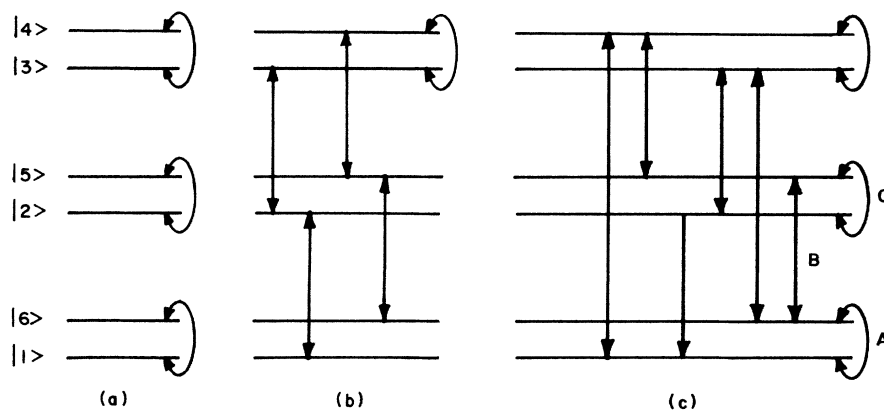
FIG. 10. Spin-relaxation transitions allowed by three different relaxation models. Electronic transitions between the six Kramer levels are shown for (a) a two-state effective-field flipping model, (b) a Blume-Tjon effective-field flipping model, and (c) a Clauser-Blume nonadiabatic spin-relaxation model.

Kramers levels and is responsible for the occurrence of the line at position 6′ in the spectrum. This process transfers energy between the ground-state Kramers doublets $|1\rangle$, $|6\rangle$, as shown in Fig. 10(c), and $|4\rangle$, $|5\rangle$. The line at position 1′ indicates a transfer of energy within the intermediate-energy Kramers doublet, levels $|4\rangle$ and $|5\rangle$.

It is interesting to note that modes A and C were not identified as occurring in TPDC[Fe(III)] in a previous study which was based solely on transmission results.[34] From our SEDM results, it is clear that mode A is dominant at low temperatures and mode C becomes important as the population of the intermediate Kramers levels increases at higher temperatures. This is not the case in FA, as was determined from earlier SEDM and transmission experiments.[21,24]

In order to understand the different dynamic behavior of the two paramagnets FA and TPDC[Fe(III)], we need to obtain a clearer picture of the interplay between the static structural parameters and the dynamic parameters which govern the behavior of paramagnetic systems. Let us concentrate on three parameters: the Kramers-level population P_i, the relaxation rate within the ground level Ω_{16}, and the relaxation rate between the lowest doublets Ω_{15}. These parameters are functions of D, λ, and T. We consider two cases, one with $D = -0.25$ cm^{-1} (case 1) representing a hypothetical compound similar to FA, and

the other with $D = -2.5$ cm^{-1} (case 2) representing a compound similar to TPDC[Fe(III)]. We will consider both weak coupling or slow relaxation with $\Omega \leq \Gamma$, and strong coupling or fast relaxation with $\Omega \gg \Gamma$. Specifically, calculations were performed with $\Omega = 1$ and $\Omega = 100$ in units of the natural linewidth.

Figures 11(a) and 11(b) give the electronic-level population of the doublets, P_i, as a function of temperature as determined by the Boltzmann factor in Eq. (23). Clearly, the ground Kramers doublet must contribute in a dominant way to the Mössbauer spectrum at low temperatures when $D = -2.50$ cm^{-1}. Even at 10 K, the population of the ground-level doublet is more than three times the population of the other two doublets. On the other hand, for the case $D = -0.25$ cm^{-1} at 10 K, the level population of the three doublets does not differ by more than 15%. Thus, one expects intradoublet relaxation to play a major role in case 2, but not in case 1, over the temperature range 1.0 to 10 K. This is confirmed by the calculated results shown in Figs. 12 and 13 where the effective relaxations T_{16} and T_{15} for these two cases are plotted.

For $D = -0.25$ cm^{-1} and $\lambda = \frac{1}{3}$, at temperatures down to about 2 K, the dominant relaxation mode transfers energy between Kramers doublets [mode B in Fig. 10(c) for both slow relaxation ($\Omega = 1.0$) and fast relaxation ($\Omega = 100$)]. This occurs because $T_{15} > T_{16}$, as can be seen
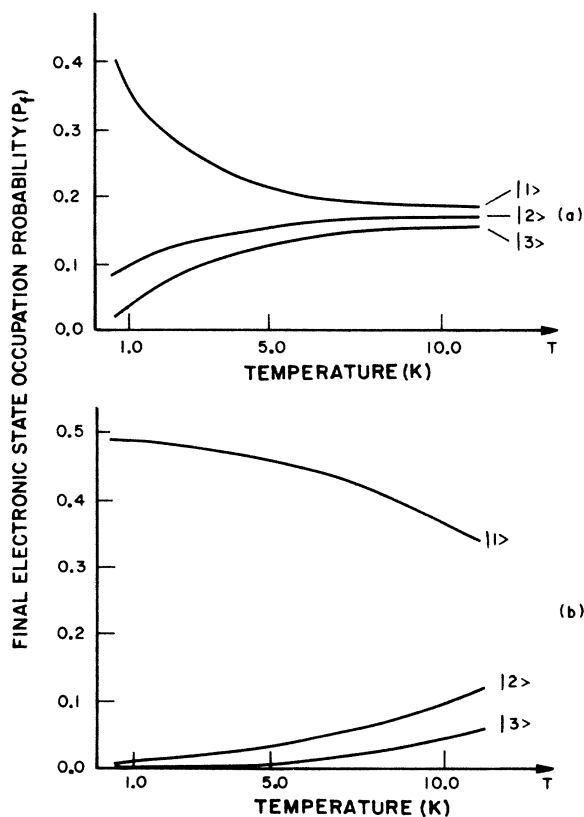
FIG. 11. Population of different Kramers levels as a function of temperature for (a) $D = -0.25$ cm^{-1} and (b) $D = -2.5$ cm^{-1}, $\lambda = \frac{1}{3}$ and the curves are labeled according to the convention introduced in Fig. 10, so that 1 and 6 are the ground-state levels with $D < 0$.
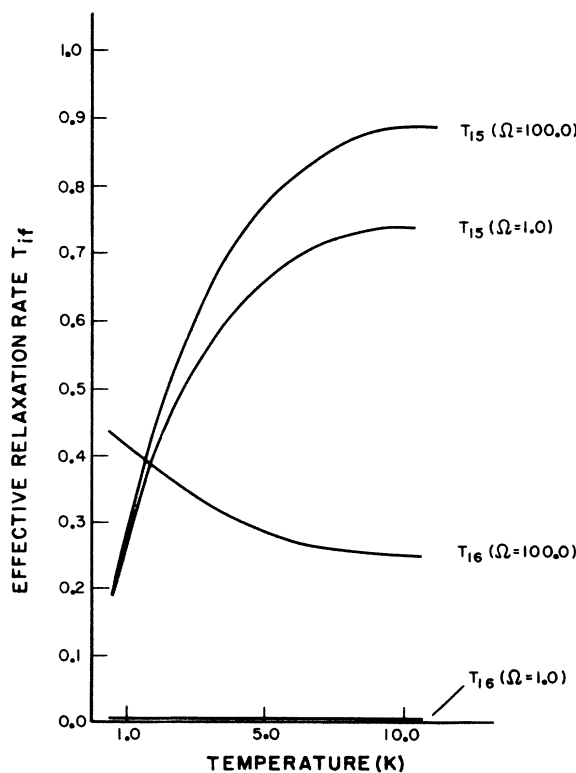
FIG. 12. Effective relaxation rate T_{16} and T_{15} [as defined by Eq. (24)] between levels of the ground Kramers doublet and the ground doublet and first excited level, respectively, plotted as a function of temperature for two values of the base relaxation rate $\Omega = 1.0$ and $\Omega = 100$ (in units of the natural linewidth) for $\lambda = \frac{1}{3}$ and $D = -0.25$ cm^{-1}.
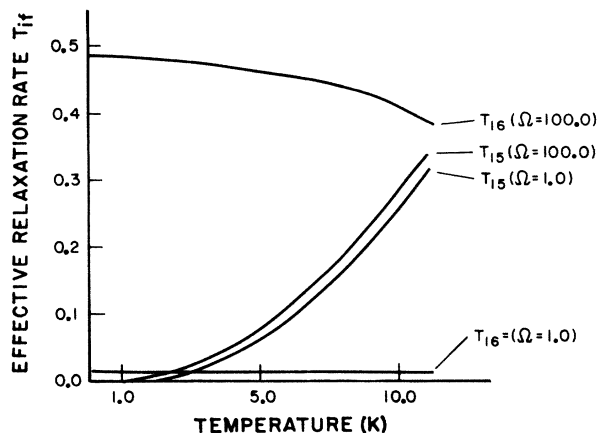
FIG. 13. Effective relaxation rates T_{16} and T_{15} between levels of the ground Kramers doublet and the ground doublet and first excited level, respectively, plotted as a function of temperature for two values of the base relaxation rate $\Omega = 1.0$ and $\Omega = 100$ (in units of natural linewidth) and for $\lambda = \frac{1}{3}$ and $D = -2.5$ cm^{-1}.

from Fig. 12. Relaxation of this type was observed in FA in both Mössbauer transmission[24] and SEDM (Ref. 21) experiments. For $D = -2.5$ cm^{-1}, the situation changes markedly for fast relaxation ($\Omega = 100$), as can be seen from Fig. 13. In this latter case, relaxation within the ground Kramers doublet dominates [mode A in Fig. 10(c) since $T_{16} > T_{15}$ for low temperatures below 10 K].

The relaxation mechanism depicted in Fig. 10(c) and Fig. 13 is, in general, consistent with our experimental results on TPDC[Fe(III)]. Transfer of energy between the energy levels of the Kramers ground doublet, $|1\rangle$ and $|6\rangle$, was determined to exist at $T = 5.4$ K by the appearance of the peak at the position of the No. 1 resonance peak after excitation of the No. 6 resonance peak (Fig. 7). At $T = 8$ K the appearance of the other two lines in the experimental SEDM spectrum (Fig. 8) shows the existence of relaxation between the ground state, $|1\rangle$ and $|6\rangle$, and intermediate, $|2\rangle$ and $|5\rangle$, Kramers doublets, as well as within the intermediate doublet, $|2\rangle$ and $|5\rangle$, and the ground-state doublet $|1\rangle$ and $|6\rangle$.

A schematic picture of the relaxation processes occurring in TPDC[Fe(III)] is shown in Fig. 10(c). The arrows labeled A, B, and C indicate the transitions actually observed in our SEDM experiments. A fit of the SEDM theoretical spectra to the experimental results provided the relaxation rates Ω_{ij}. Spectra calculated from Eqs. (1), (2), (4), and (A1), which give the best fit to our data at 5.4 and 8.0 K, are given by solid lines in Figs. 7 and 8. For

the calculations, we used $\beta_s = 300$, $\beta_a = 14$, which was determined by the ^{57}Fe content in the sample and the single-line absorber, respectively, and $\Gamma_b = 2.4$, as determined from the experiment on the natural metal (Fig. 5). Thus, the calculations were performed without any free parameters except for the normalization factor which was determined from the best fit at the excitation energy (indicated by the vertical arrows in the figures). The results are summarized in Table I, where the relaxation rates are given in units of the natural linewidth Γ.

From the results given in Table I, the strength of the interaction or "bare" relaxation rate Ω can be obtained if D and λ are known. Using $D = -2.1$ cm^{-1} (Ref. 34) and assuming $\lambda = \frac{1}{3}$, which gives the maximum admixture of states, we get $\Omega = 512$ in units of the natural linewidth or 5.24×10^9 sec^{-1}, which is about 50 times greater than the value obtained from previous transmission studies of this compound (Ref. 34). [Our Eq. (23) is a more general form of Eq. (10)(Ref. 34) with the coupling constant C replaced by our bare relaxation rate Ω.] For smaller values of λ even larger bare relaxation rates would be required to fit the data. (For the case $\lambda = 0.25$, above relaxation rate an order of magnitude larger would be required to explain the data.) In the extreme case $\lambda = 0$, the relaxation mechanism described by Eqs. (20)–(23) would give $\Omega_{16} = 0$ and thus would not explain the lines on the extreme left of the SEDM spectra shown in Figs. 12 and 13 to first order. Clearly, an independent determination of λ is required to tie down the coupling constant. Comparing our results with earlier findings for FA (Ref. 24), where the bare relaxation rate $\Omega = 1.32$ in units of the natural linewidth or 1.35×10^7 sec^{-1} was obtained, we conclude that relaxation in FA is consistent with the weak-coupling picture or slow relaxation with $\Omega \simeq \Gamma$, whereas relaxation in TPDC[Fe(III)] is consistent with the strong-coupling picture or fast relaxation with $\Omega > \Gamma$.

VII. CONCLUSIONS

It seems clear from the calculations and experimental results presented here that SEDM experiments, together with superoperator line-shape theory, can provide detailed information about electronic and molecular dynamics. Our results show that SEDM determines directly the dynamic paths of the relaxation processes occurring in the sample by measuring the energy of the scattered radiation which is modulated by the processes in the sample. This information may be difficult if not impossible to obtain by other techniques.

In the case of TPDC[Fe(III)], we found that at 5.4 K there is one predominant relaxation path which simulates a "spin-flip" in the ground Kramers level. This mecha-

TABLE I. Relaxation parameters for TPDC[Fe(III)] obtained from theoretical fits to experimental data. (Relaxation rates Ω_{ij} given in units of the natural linewidth.)

	$\Omega_{16}(A)$	T_{16}	$\Omega_{15}(B)$	T_{15}	$\Omega_{52}(C)$	T_{52}
$T = 5.4$	4.5 ± 0.3	0.82	0	0	0	0
$T = 8.0$	4.0 ± 1.0	0.80	768	0.144	649	0.99

nism has not been observed heretofore with other techniques, such as Mössbauer transmission experiments, because of their insensitivity to differences produced in line shapes by various relaxation mechanisms (see Sec. III).

At 8.0 K we again measured with SEDM the spin-flip transition within the ground-state Kramers doublet. However, at this temperature we also measured a relaxation between the ground-state doublet and the intermediate doublet and another spin-flip transition within the intermediate doublet. These observations force a new interpretation of relaxation in TPDC[Fe(III)], as shown in Fig. 10(c) which is still consistent with the Clauser-Blume theory.

Our results indicate that SEDM is a powerful tool for relaxation studies, even with the presently available, rather weak, natural sources of Mössbauer radiation. With the advent of stronger Mössbauer sources, possibly from filtered synchrotron radiation[55] and γ-ray lasers,[56] such experiments will become much more practical even with unenriched samples.

ACKNOWLEDGMENTS

APPENDIX

The effective-field-reversal model permits a closed-form expression of the SEDM line shape for all values of the relaxation rate. In this model there is no coupling between the outer two lines of the spectrum and the four inner lines. The field reversal merely interchanges the energies of the nuclear levels (see Ref. 22, Fig. 9). The smallest independent subsystem for describing this process in ^{57}Fe is composed of four nuclear substates ($\pm\frac{1}{2}$ for both excited and ground states) and two electronic states ($+,-$) as depicted in Fig. 14. All the possible transitions between the four nuclear energy levels are given by the transiton matrix elements J_i. The only thing that has to be provided now to permit the line-shape calculation is the form of the relaxation matrix W, which determines the relaxation mechanism. For our two-state electronic system, the relaxation superoperator matrix elements $\langle \alpha,\beta \,|\, S \,|\, \gamma,\delta \rangle$ are[32]

	$++$	$--$	$+-$	$-+$
$++$	$-\Omega_1$	Ω_1	0	0
$--$	Ω_1	$-\Omega_1$	0	0
$+-$	0	0	$-\Omega_2$	0
$-+$	0	0	0	$-\Omega_2$

The three terms in Eq. (11) can now be obtained in closed form for this eight-state, nuclear-electronic system depicted in Fig. 14. Assuming $\Omega_1 = \Omega_2$, these terms are given by
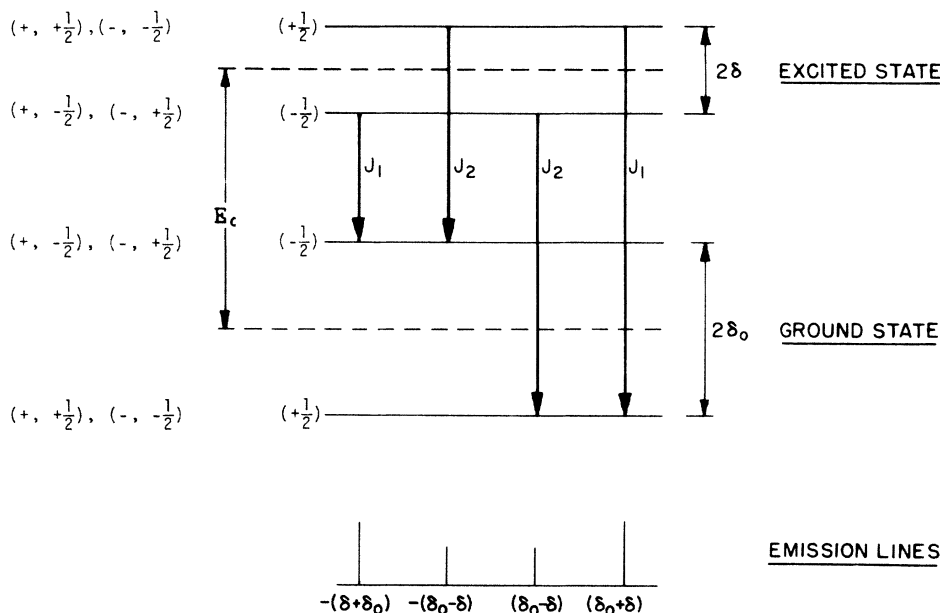
FIG. 14. Energy levels and allowed transitions for the eight-state system. The two electronic states are labeled $+$ and $-$ and the four nuclear substates $+\frac{1}{2}$ and $-\frac{1}{2}$ where values of $\frac{3}{2}$ for the excited state and $\frac{1}{2}$ for the ground state are assumed.

$$I_1 = \sum_{a,b,c,d=1}^{2} \{ [J_a^2 J_c^2 \alpha_{ba} \beta_{xy} \gamma_{bc}$$

$$+ J_b^2 J_d^2 \alpha_{ba} \beta_{xz} \gamma_{dc}](1 - \delta_{bd}) \} ,$$

$$I_2 = \sum_{a,b,c,d=1}^{2} \{ (1 - \delta_{bd})[\epsilon_{d1}\alpha_{ba} + \theta_1 \alpha_{da}] \gamma_{bc}^* J_a^2 J_c^2$$

$$+ (1 - \delta_{bd})[\epsilon_{d2}\alpha_{ba} + \theta_2 \alpha_{da}] \gamma_{bc}^* J_b^2 J_d^2 \} , \qquad \text{(A1)}$$

$$I_3 = \sum_{a,b,c,d=1}^{2} \{ (1 - \delta_{bd})[\epsilon_{d1}\alpha_{ba} + \theta_1 \alpha_{da}] \gamma_{bc} J_a^2 J_c^2$$

$$+ (1 - \delta_{bd})[\epsilon_{d2}\alpha_{ba} + \theta_2 \alpha_{da}] \gamma_{dc} J_b^2 J_d^2 \} ,$$

where

$$x = 1 + \delta_{ab}, \quad y = 2 - \delta_{ac}, \quad z = 1 + \delta_{ac} ,$$

$$\alpha_{ij} = \frac{a_{kj} - i\Omega}{a_{ij}a_{kj} + \Omega^2}, \quad \beta_{ij} = \frac{b_{kj} + i\Omega}{b_{ij}b_{kj} + \Omega^2} ,$$

$$\gamma_{ij} = \frac{c_{kj} + i\Omega}{c_{ij}c_{kj} + \Omega^2}, \quad \epsilon_{ij} = \frac{e_{ki}}{e_{ij}e_{kj} + \Omega^2} ,$$

$$\theta_j = \frac{-i\Omega}{e_{ij}e_{kj} + \Omega^2}, \quad i,j = 1,2 \text{ and } k \neq i ,$$

with

$$a_{ij} = E' - \Delta_{ij} - i(\Gamma/2 + \Omega) ,$$

$$b_{ij} = (E - E' - d_{ij}) + i(\Gamma_b/2 + \Omega) ,$$

$$c_{ij} = E - \Delta_{ij} + i[(\Gamma + \Gamma_b)/2 + \Omega], \quad e_{ij} = -d_{ij}' - i(\Gamma + \Omega) ,$$

and

$$\Delta_{11} = \delta - \delta_0, \quad d_{11} = d_{21} = 0 ,$$

$$\Delta_{21} = -(\delta - \delta_0), \quad d_{12} = -d_{22} = 2\delta_0 ,$$

$$\Delta_{12} = \delta + \delta_0, \quad d_{11}' = d_{21}' = 0 ,$$

$$\Delta_{22} = -(\delta + \delta_0), \quad d_{12}' = -d_{22}' = 2\delta .$$

The terms comprising Eq. (A1) are written out explicitly in Table I of Ref. 27. The eight-state, nuclear-electronic system is the basic structure unit for calculating the SEDM spectrum of ^{57}Fe in the effective-field model. Transitions J_1 and J_2 give the four inner lines (2,3,4,5) of the full six-line ^{57}Fe spectrum, as shown in Fig. 2. To obtain the outer lines, we have to include transitions between the ground-state levels $(\pm \frac{1}{2})$ and the excited levels $(\pm \frac{3}{2})$. These can be treated as a special case of the eight-state system with $J_2 = 0$, $J_1 = J_3$, where

$$J_3 = \langle \pm \tfrac{3}{2} | V | \pm \tfrac{1}{2} \rangle^2 .$$

Combining transitions J_1, J_2, and J_3 gives the total ^{57}Fe spectrum. For a degenerate nuclear ground state $(\delta_0 = 0, J_2 = 0)$, Eqs. (A1) reduce to much simpler expressions:

$$I_1 = 2J_4[(\alpha_1 + \alpha_2)(\gamma_1 + \gamma_2)]\beta ,$$

$$I_2 = 2J^4[\delta_1(\epsilon_1 + \epsilon_1')\alpha_1 + \delta_2(\epsilon_2 + \epsilon_2')\alpha_2$$

$$+ \alpha_1(\theta + \theta')\delta_2 + \alpha_2(\theta + \theta')\delta_1] ,$$

$$I_3 = -2J^4[\alpha_1(\epsilon_1\gamma_1 + \epsilon_1'\gamma_2) + \alpha_2(\epsilon_2\gamma_1 + \epsilon_2'\gamma_2)] ,$$

where

$$\alpha_i = \frac{a_j - i\Omega}{a_i a_j + \Omega^2}, \quad i = 1,2$$

(also for $\gamma_i, \delta_i, \epsilon, \epsilon'$ with a_i replaced by c_i, d_i, e_i, e_i', respectively)

$$\beta = \frac{b + i\Omega}{b^2 + \Omega^2} ,$$

$$a_{1,2} = (E' \mp \delta) - i(\Gamma/2 + \Omega) ,$$

$$c_{1,2} = (E \mp \delta) + i[(\Gamma_b + \Gamma)/2 + \Omega)] ,$$

$$d_{1,2} = (E \mp \delta) - i[(\Gamma_b + \Gamma)/2 + \Omega] ,$$

$$b = (E - E') + i(\Gamma_b/2 + \Omega) ,$$

$$e_1 = -i(\Gamma + \Omega), \quad e_2 = -i(\Gamma + \Omega) ,$$

$$e_1' = -2\delta - i(\Gamma + \Omega), \quad e_2' = +2\delta - i(\Gamma + \Omega) .$$

[1]H. H. Wickman and G. R. Wertheim, Phys. Rev. **148**, 211 (1966); and, in *Chemical Applications of Mössbauer Spectroscopy*, edited by V. I. Goldanskii and R. H. Herber (Academic, New York, 1968), p. 548.

[2]G. Lang and W. Marshall, Proc. Phys. Soc. London **87**, 3 (1966).

[3]K. Spartalian, in *Advances in Mössbauer Spectroscopy Applications to Physics, Chemistry and Biology*, edited by B. V. Thosar, P. K. Iyengar, J. K. Srivastava, and S. C. Bhargava (Elsevier Scientific, New York, 1983), Chap. 8, pp. 455–486.

[4]E. R. Bauminger, S. G. Cohen, E. Giberman, I. Nowik, and S. J. Ofer, J. Phys. (Paris) Colloq. **37**, C6-227 (1976).

[5]H. J. Ubelhack and F. H. Wittmann, J. Phys. (Paris) Colloq. **37**, C6-269, 1976.

[6]H. Winkler, H. J. Heinrich, and E. Gerdau, Phys. (Paris) Colloq. **37**, C6-26 (1976).

[7]J. A. Tjon and M. Blume, Phys. Rev. **165**, 456 (1968).

[8]W. Kundig and R. S. Hargrove, Solid State Commun. **223**, 7 (1969).

[9]B. Balko and G. R. Hoy, J. Phys. (Paris) Colloq. **37**, C6-89 (1976).

[10]I. P. Dzub and A. F. Lubchenko, Fiz. Tverd. Tela **3**, 2275 (1961) [Sov. Phys.—Solid State **3**, 1651 (1962)].

[11]J. E. Knudsen and S. Morup, Proceedings of International Conference on Mössbauer Spectroscopy, Bucharest, Romania, 1977 (unpublished).

[12]A. J. F. Boyle and J. R. Gabriel, Phys. Lett. **19**, 451 (1965).

[13]F. Van der Woude, Phys. Status Solidi **17**, 417 (1966).

[14]G. K. Shenoy, B. D. Dunlap, S. Dattagupta, and L. Asch, Phys. Rev. Lett. **37**, 539 (1976); S. Dattagupta, Phys. Rev. B

12, 3584 (1975).

[15]G. R. Hoy and M. R. Corson, J. Magn. Magn. Mater. 627, 15 (1980).

[16]G. R. Hoy and M. R. Corson, in *Mössbauer Spectroscopy and Its Chemical Applications,* edited by J. G. Stevens and G. K. Shenoy (American Chemical Society, Washington, D.C., 1981), Chap. 21, p. 463.

[17]S. L. Ruby and J. M. Hicks, Rev. Sci. Instrum. 33, 27 (1962).

[18]S. Margulies and J. R. Ehrman, Nucl. Instrum. Methods 12, 131 (1961).

[19]A. M. van Diepen, 2C3, International Conference on Magnetism, Amsterdam, 1976 (unpublished).

[20]P. P. Wintersteiner, Ph.D. dissertation, Boston University, 1976.

[21]B. Balko, E. V. Mielczarek, and R. L. Berger, in *Frontiers of Biological Energetics: From Electrons to Tissues,* edited by P. L. Dutton, J. S. Leigh, and A. Scarpa (Academic, New York, 1979), Vol. I, p. 617.

[22]H. H. Wickman, M. P. Klein, and D. A. Shirley, Phys. Rev. 152, 345 (1966).

[23]B. Balko, E. V. Mielczarek, and R. L. Berger, J. Phys. (Paris) Colloq. 40, C2-17 (1972).

[24]G. R. Hoy, M. Corson, and B. Balko, Phys. Rev. B 27, 2652 (1983).

[25]B. Balko and G. R. Hoy, Phys. Rev. B 10, 36 (1974).

[26]B. Balko and G. R. Hoy, in *Mössbauer Effect Methodology,* edited by I. J. Gruverman (Plenum, New York, 1974), Vol. 9.

[27]B. Balko and G. R. Hoy, *Mössbauer Spectroscopy: Applications in Physics, Chemistry and Biology,* edited by B. V. Thosar, P. K. Iyengar, J. K. Srivastava, and S. C. Bhargava (Elsevier Scientific, New York, 1983), Chap. 8, pp. 455–486.

[28]B. Balko and G. R. Hoy, Phys. Lett. 47A, 171 (1973).

[29]B. Balko and G. R. Hoy, Physica 86—88B, 953 (1977).

[30]B. Furubayashi and I. Sakamoto, J. Phys. (Paris) Colloq. 40, C2-677 (1979).

[31]A. M. Afanasev and B. D. Gorobchenko, Zh. Eksp. Teor. Fiz. 67, 2246 (1975)[Sov. Phys.—JETP 40, 1114 (1975)].

[32]F. Hartmann-Boutron, J. Phys. 37, 537 (1976).

[33]S. Banarjee, Ph.D. dissertation, State University of New York at Stony Brook, 1977; Phys. Rev. B 19, 5463 (1979).

[34]H. H. Wickman and C. F. Wagner, J. Chem. Phys. 51, 435 (1969).

[35]B. Balko, Ph.D. dissertation, Boston University, 1973.

[36]D. G. Klissurski and I. G. Mitov, J. Phys. (Paris) Colloq. 40, C2-353 (1979).

[37]B. H. Huynh, E. Munck, and W. H. Orme-Johnson, J. Phys. (Paris) Colloq. 40, C2-526 (1979).

[38]B. Balko and G. R. Hoy, Phys. Rev. B 13, 2729 (1976).

[39]J. P. Hannon and G. T. Trammell, Phys. Rev. 169, 315 (1968); 186, 306 (1969); J. P. Hannon, N. J. Carron, and G. T. Trammell, Phys. Rev. B 9, 2810 (1974).

[40]Yu. Kagan, A. M. Afanasav, and I. P. Perstnev, Zh. Eksp. Teor. Fiz. 54, 1530 (1968) [Sov. Phys.—JETP 27, 819 (1968)].

[41]Yu. Kagan and A. M. Afanasev, Zh. Eksp. Teor. Fiz. 49, 1504 (1965) [Sov. Phys.—JETP 22, 1032 (1966)].

[42]D. C. Champeney, Rep. Prog. Phys. 42, 1016 (1979).

[43]J. P. Hannon and G. T. Trammell, Optics Commun. 15, 330 (1975).

[44]J. H. Terhune and G. C. Baldwin, Phys. Rev. Lett. 14, 589 (1965).

[45]F. E. Wagner, J. Phys. (Paris) Colloq. 37, C6-673 (1976).

[46]B. Balko and G. R. Hoy, Phys. Rev. B 10, 4523 (1974).

[47]W. Heitler, *Quantum Theory of Radiation* (Clarendon, Oxford, 1954), pp. 196—204.

[48]A. J. F. Boyle and H. E. Hall, Rep. Prog. Phys. 25, 455 (1962).

[49]M. Blume, Phys. Rev. 174, 351 (1968).

[50]S. Dattagupta, Phys. Rev. B 16, 158 (1977).

[51]M. J. Clauser and M. Blume, Phys. Rev. B 3, 583 (1971).

[52]Y. R. Shen, Phys. Rev. B 9, 622 (1974).

[53]Y. Toyogawa, A. Kotani, and A. Sumi, J. Phys. Soc. Jpn. 42, 1495 (1977).

[54]S. Dattagupta, Phys. Rev. B 12, 3584 (1975).

[55]J. P. Hannon, Bull. Am. Phys. Soc. 27, 453 (1982).

[56]G. C. Baldwin, J. C. Solem, and V. I. Goldanskii, Rev. Mod. Phys. 53, 687 (1981).